

Article

Ratiometric Fluorescence Detection of Colorectal Cancer-Associated Exosomal miR-92a-3p with DSN-Assisted Signal Amplification by a MWCNTs@Au NCs Nanoplatfrom

Zhiwei Sun ^{1,2}, Juan Li ³, Yao Tong ³, Li Zhao ¹, Xiaoyu Zhou ¹, Hui Li ¹, Chuanxin Wang ^{3,4,5}, Lutao Du ^{3,*} and Yanyan Jiang ^{1,2,*}

- ¹ Key Laboratory for Liquid–Solid Structural Evolution and Processing of Materials, Ministry of Education, Shandong University, Jinan 250061, China; sun_zhiwei@mail.sdu.edu.cn (Z.S.); 202020473@mail.sdu.edu.cn (L.Z.); zhouxiaoyu322@163.com (X.Z.); lihuilmy@hotmail.com (H.L.)
- ² Shenzhen Research Institute of Shandong University, Shenzhen 518057, China
- ³ Department of Clinical Laboratory, The Second Hospital, Cheeloo College of Medicine, Shandong University, Jinan 250033, China; niderouke@163.com (J.L.); tooong1997@126.com (Y.T.); cxwang@sdu.edu.cn (C.W.)
- ⁴ Shandong Engineering & Technology Research Center for Tumor Marker Detection, Jinan 250033, China
- ⁵ Shandong Provincial Clinical Medicine Research Center for Clinical Laboratory, Jinan 250033, China
- * Correspondence: lutaodu@sdu.edu.cn (L.D.); yanyan.jiang@sdu.edu.cn (Y.J.); Tel.: +86-18560083207 (L.D.); Tel.: +86-17865551290 (Y.J.)

Abstract: The detection of miRNA shows great promise in disease diagnosis. In this work, a ratiometric fluorescent biosensor based on multi-walled carbon nanotubes@gold nanoclusters (MWCNTs@Au NCs) and duplex-specific nuclease (DSN)-assisted signal amplification was fabricated for miRNA detection. Colorectal cancer (CRC)-associated miR-92a-3p extracted from exosomes was selected as the target. MWCNTs@Au NCs performs the dual functions of fluorescence quencher and internal fluorescence reference. In the absence of miR-92a-3p, an Atto-425-modified single-stranded DNA probe is adsorbed on MWCNTs@Au NCs, resulting in the quenching of Atto-425. In the presence of miR-92a-3p, the duplex is formed by hybridization of the probe and miR-92a-3p and leaves the MWCNTs@Au NCs, resulting in the fluorescence recovery of Atto-425. DSN can cleave the probe and result in the release of miR-92a-3p. The released miR-92a-3p can hybridize with other probes to form a signal amplification cycle. The fluorescence of MWCNTs@Au NCs remains stable and constitutes a ratiometric fluorescence system with that of Atto-425. A detection concentration interval of 0.1–10 pM and a limit of detection of 31 fM was obtained under optimized measurement conditions. In addition, the accuracy of the biosensor was validated by detecting the concentration of miR-92a-3p extracted from clinical exosome samples.

Keywords: multi-walled carbon nanotubes; Au nanoclusters; biosensor; ratiometric fluorescence; duplex-specific nuclease; exosomal miRNA



Citation: Sun, Z.; Li, J.; Tong, Y.; Zhao, L.; Zhou, X.; Li, H.; Wang, C.; Du, L.; Jiang, Y. Ratiometric Fluorescence Detection of Colorectal Cancer-Associated Exosomal miR-92a-3p with DSN-Assisted Signal Amplification by a MWCNTs@Au NCs Nanoplatfrom. *Biosensors* **2022**, *12*, 533. <https://doi.org/10.3390/bios12070533>

Received: 6 June 2022
Accepted: 15 July 2022
Published: 17 July 2022

Publisher's Note: MDPI stays neutral with regard to jurisdictional claims in published maps and institutional affiliations.



Copyright: © 2022 by the authors. Licensee MDPI, Basel, Switzerland. This article is an open access article distributed under the terms and conditions of the Creative Commons Attribution (CC BY) license (<https://creativecommons.org/licenses/by/4.0/>).

1. Introduction

MicroRNAs (miRNAs) are small, single-stranded, noncoding RNAs of 18–24 nucleotides that play key roles in many biological processes, including cell proliferation, differentiation, stress resistance and apoptosis by regulating gene expression at the post-transcriptional level [1–3]. Numerous studies have found that changes in miRNA expression are closely related to the occurrence of various diseases, such as cardiovascular disease, obesity, diabetes and tumors [4–7]. Therefore, detection of the expression level of miRNAs in organisms can provide valuable information for biomedical research and early disease diagnosis [8,9]. Based on this, the exploitation of fast, sensitive and selective sensing strategies for miRNAs has attracted immense interest.

Effective detection of miRNAs is challenging due to their small size, low expression level and high sequence similarity [10,11]. Recently, several signal amplification strategies,

including real-time quantitative polymerase chain reaction (RT-qPCR), hybridization chain reaction, rolling circle amplification, nicking enzyme and duplex-specific nuclease (DSN), have been developed to improve the detection sensitivity for miRNA [12–16]. Further, miRNA biosensing based on DSN-assisted signal amplification is considered a promising strategy. DSN-amplified miRNA detection has been known for a decade, and since then there have been many examples reported [17]. DSN can cleave DNA in DNA–RNA heteroduplexes into DNA fragments while keeping the RNA strand intact, which indicates that the complete miRNA target can be reused to form a new heteroduplex structure for the next step of cleavage [18,19]. DSN cleavage of those duplexes with more than 10–12 base complementary pairs ensures the high selectivity for the target [20]. Meanwhile, fluorescence-based detection methods are commonly used in bioassays because of their excellent sensitivity and rapid analysis [21,22]. Based on the above merits, the combination of DSN-assisted target cyclic signal amplification and fluorescence-based detection can achieve sensitive, selective and fast detection of miRNA.

Fluorescence-quenching nanomaterials such as Mxenes, graphene oxide, g-C₃N₄, MoS₂, gold nanoparticles (Au NPs) and multi-walled carbon nanotubes (MWCNTs) have been widely used in biosensing [23–28]. Among them, MWCNTs have a large adsorption surface and can act as an excellent substrate for the preparation of MWCNT-based nanocomposites [29–31]. For instance, in the work of Ma et al., MWCNTs were used as an excellent fluorescence quenching platform for the detection of miRNA-155 in human serum [30]. The synthesized MWCNT/Au NPs showed a quenching efficiency of 93.2% for a FAM-labeled single-stranded DNA probe, paving the way for the sensitive detection of miRNA-155. However, the reliability of this detection strategy, which relies on a single fluorophore, is easily disturbed by unstable factors such as the light source and complex solution environment [32,33]. To overcome this limitation, ratiometric fluorescence biosensing has received increasing attention due to its capability to counteract the effects of instabilities [34–36].

In this work, we successfully synthesized multi-walled carbon nanotubes@gold nanoclusters (MWCNTs@Au NCs) with dual functions of fluorescence emission and quenching by linking Au NCs to MWCNTs through Au–S bonds. A sensitive and selective ratiometric fluorescent biosensor based on MWCNTs@Au NCs and DSN-assisted signal amplification was fabricated for miRNA detection. Colorectal cancer (CRC)-associated miR-92a-3p extracted from exosomes served as the target in view of its high abundance in exosomes [37]. The morphology, surface properties and optical characteristics of MWCNTs@Au NCs were firstly analyzed. Then, the fluorescence signals of the biosensing system were measured, and the feasibility of biosensing was verified. Subsequently, the measurement conditions of the biosensor were optimized, and the sensitivity and selectivity of detection were explored. Finally, we validated the accuracy of the proposed biosensor in the detection of miR-92a-3p extracted from exosomes by RT-qPCR.

2. Materials and Methods

2.1. Samples and Materials

All serum samples were obtained from healthy controls and CRC patients at the Second Hospital of Shandong University. This work was approved by the ethics committee of the Second Hospital of Shandong University.

Tetrachloroauric(III) acid tetrahydrate (HAuCl₄·4H₂O, AR grade), glutathione reduced (C₁₀H₁₇N₃O₆S, ≥98%), β-mercaptoethylamine (C₂H₇NS, 98%), concentrated sulfuric acid (H₂SO₄, GR grade) and concentrated nitric acid (HNO₃, AR grade) were purchased from Sinopharm Chemical Reagent Co., Ltd. Multi-wall carbon nanotubes (ID: 5–10 nm, OD: 30–50 nm, length: <10 μm), N-(3-dimethylaminopropyl)-N'-ethylcarbodiimide hydrochloride (EDC; C₈H₁₈ClN₃, 98.5%), N-hydroxysuccinimide (NHS; C₄H₅NO₃, 99%), Tris-HCl buffer (1 M, pH 7.4) and MES buffer (0.5 M, pH 5.5) were purchased from Shanghai Macklin Biochemical Co., Ltd. (Shanghai, China). DSN was purchased from Evrogen JSC. The probe was purchased from Sangon Biotech (Shanghai) Co., Ltd. (Shanghai, China). The

miR-92a-3p and mismatched sequences were purchased from Shanghai Genepharma Co., Ltd. (Shanghai, China). Ultrapure water was used in all experiments. All oligonucleotide sequences are listed in Table 1.

Table 1. The oligonucleotide sequences used in this work.

Oligonucleotide	Sequence (5' → 3')
Probe miR-92a-3p	Atto-425-(CH ₂) ₆ -ACAGGCCGGGACAAGTGCAATA UAUUGCACUUGUCCCGGCCUGU
Single base mismatched target (SMT)	UAUUCCACUUGUCCCGGCCUGU
Two base mismatched target (TMT)	UUUUCCACUUGUCCCGGCCUGU
Non-complementary target (NCT)	UGUCAGUUUGUCAAAUACCCCA

2.2. Synthesis of Fluorescent Au NCs

Firstly, 10 mL tetrachloroauric(III) acid tetrahydrate aqueous solution (4 mM) was added to a three-necked flask and stirred at 25 °C for 5 min under a nitrogen atmosphere. Then, 10 mL glutathione reduced aqueous solution (6 mM) was injected and stirred for 10 min. Subsequently, the solution was refluxed at 100 °C for 12 h. The purified Au NCs aqueous solution was obtained by dialysis with ultrapure water for 24 h.

2.3. Preparation of MWCNTs@Au NCs

For carboxylation of MWCNTs [38], MWCNTs (0.1 g) were added to 20 mL of a mixture of concentrated sulfuric acid and concentrated nitric acid (3:1 by volume) and sonicated for 4 h. Then, the mixture was centrifuged and washed repeatedly with ultrapure water and dried at 60 °C for 12 h to obtain carboxylated MWCNTs.

For conjugation of Au NCs and MWCNTs, MWCNTs (10 mg), MES buffer (20 µL; 0.5 M, pH 5.5), EDC (10 mg) and NHS (10 mg) were dispersed in 10 mL ultrapure water and stirred at 30 °C for 0.5 h to activate the carboxyl of the MWCNTs. Next, Tris-HCl buffer (200 µL; 1 M, pH 7.4) and β-mercaptoethylamine (10 mg) were added and stirred for 12 h. Subsequently, the solution was dialyzed with ultrapure water for 24 h to obtain thiol-modified MWCNTs. Finally, 10 mL Au NCs aqueous solution (0.39 mg/mL) was added to the above solution and stirred for 24 h to obtain MWCNTs@Au NCs. The concentration of MWCNTs@Au NCs was calculated to be 0.7 mg/mL by weighing the mass of the MWCNTs@Au NCs collected by freeze-drying.

2.4. Fluorescence Detection of miR-92a-3p

Probe (1 µL, 10 µM) and Tris-HCl buffer (10 µL; 1 M, pH 7.4) were added to MWCNTs@Au NCs solution (100 µL, 0.7 mg/mL) and maintained at 25 °C for 40 min. Then, the target (5 µL) with different concentrations, DSN master buffer (10 µL, used as obtained) and DSN (0.2 µL) were added and incubated at 45 °C for 2 h. After that, DSN stop solution (5 µL, 10 mM EDTA) was added and kept for 10 min to inactivate DSN. The solution volume was quantified to 2 mL by adding ultrapure water. The fluorescence intensities were collected using a fluorescence spectrophotometer. The excitation wavelength was 430 nm, and the slits for both excitation and emission were set to be 15 nm. The fluorescence spectra in the range of 465–700 nm were collected. All measurements were performed in parallel three times, and the averages were reported.

2.5. Extraction of Exosomes and Exosomal RNAs

ExoQuick™ Exosome Precipitation Solution (System Biosciences, Los Angeles, CA, USA) was used to extract exosomes from 0.3 mL serum according to the manufacturer's protocols. The marker proteins CD63 and CD9 of exosomes were analyzed by Western blotting. Total RNAs of exosomes were extracted by miRNeasy Micro Kit (50) (Qiagen, Dusseldorf, Germany) according to the manufacturer's instruction. Total RNA solution was quantified to 30 µL by adding ultrapure water.

2.6. Characterization

The morphology of MWCNTs, MWCNTs@Au NCs and exosomes were observed by a transmission electron microscope (TEM; HT7700, Hitachi). The zeta potentials of MWCNTs and MWCNTs@Au NCs were measured by a zeta potential analyzer (Zetasizer NanoZS, Malvern). The Fourier transform infrared spectra (FTIR) of MWCNTs and MWCNTs@Au NCs were collected by a Fourier transform infrared spectrometer (Tensor 37, Bruker). The fluorescence properties of MWCNTs@Au NCs were measured by a fluorescence spectrophotometer (RF-6000, Shimadzu). The ultraviolet–visible (UV–vis) absorption spectra of MWCNTs and MWCNTs@Au NCs were collected by an ultraviolet–visible spectrophotometer (Specord 200 plus, Analytikjena).

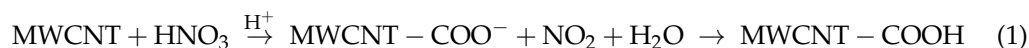
2.7. RT-qPCR Detection of miR-92a-3p

RT-qPCR was used as the reference to test the accuracy of the ratiometric fluorescent biosensor. A total of 3.75 μL of RNAs were reverse transcribed by Mir-X™ miRNA First-Strand Synthesis (Takara, Kusatsu, Japan) on T100™ Thermal Cycler (Bio-Rad, Shanghai, China) to synthesize cDNAs. RT-qPCR was carried out by SYBR® Green Premix Pro Taq HS qPCR Kit AG11701 (Accurate Biology, Shanghai, China) on a CFX96™ Real-Time System (Bio-Rad, China). The calibration line was drawn based on the real-time fluorescence curves obtained at different concentrations of miR-92a-3p.

3. Results and Discussion

3.1. Characterization of Materials

MWCNTs@Au NCs were synthesized following the procedure illustrated in Figure 1a. First, MWCNTs were carboxylated by concentrated sulfuric acid and concentrated nitric acid according to Equation (1), and the water solubility of the MWCNTs was improved by carboxylation [39]. Then, the carboxyl groups of the MWCNTs were activated by EDC and NHS, and the sulfhydryl groups were modified onto MWCNTs by amidation of the carboxyl groups with the amino groups of the β -mercaptoethylamine. Finally, the sulfhydryl groups of MWCNTs and Au NCs formed Au–S bonds via incubation. The morphologies of MWCNTs, Au NCs and MWCNTs@Au NCs were observed by TEM. As shown in Figure 1b, the hollow MWCNTs display outer diameters of 30–50 nm and are well dispersed in water. The prepared Au NCs with glutathione as a reducing agent show a size range of 2–3.5 nm and good monodispersity in water (Figure 1c). For the preparation of MWCNTs@Au NCs, thiol was firstly modified on the carboxylated MWCNTs by amidation. Then, Au–S bonds were formed between MWCNTs and Au NCs by adding Au NCs and reacting for 24 h. The TEM image of MWCNTs@Au NCs demonstrates that dense Au NCs are uniformly distributed on MWCNTs (Figure 1d,e). The absence of monodispersed Au NCs in MWCNTs@Au NCs solution indicates that the Au NCs are fully conjugated to MWCNTs.



Conjugation between MWCNTs and Au NCs was further confirmed by FT-IR analysis. As can be seen from Figure 2a, a distinct characteristic band around 1710 cm^{-1} attests to carboxyl existing in the spectrum of MWCNTs, implying that the MWCNTs are rich in carboxyl. In the spectrum of MWCNTs@Au NCs, a characteristic band at 3765 cm^{-1} attributed to amide appears, while that of carboxyl disappears, indicating that the β -mercaptoethylamine has been modified onto MWCNTs. In addition, a characteristic band at 1645 cm^{-1} appeared in the spectrum of MWCNTs@Au NCs, demonstrating the successful conjugation of MWCNTs and Au NCs [40]. The zeta potential of MWCNTs is -28.3 mV due to its surface rich in carboxyl and hydroxyl (Figure 2b). This means that MWCNTs have excellent water dispersibility. MWCNTs@Au NCs shows more negative zeta potential of -36.7 mV , indicating that it has better water dispersibility than MWCNTs. Despite the fluorescence-quenching performance of MWCNTs, the MWCNTs@Au NCs still emit intense red fluorescence under excitation at 360 nm, as depicted in the inset of

Figure 2c. The fluorescence emission peak of MWCNTs@Au NCs is located at 625 nm, and its fluorescence intensity decreases with increasing excitation wavelength. In the UV–vis absorption spectrum of MWCNTs, there is a typical carbon skeleton absorption peak located at 200–300 nm (Figure 2d). The absorbance of MWCNTs@Au NCs decreases with the increase of irradiation wavelength, which is attributed to the weakening of the plasmonic resonance of Au NCs [41].

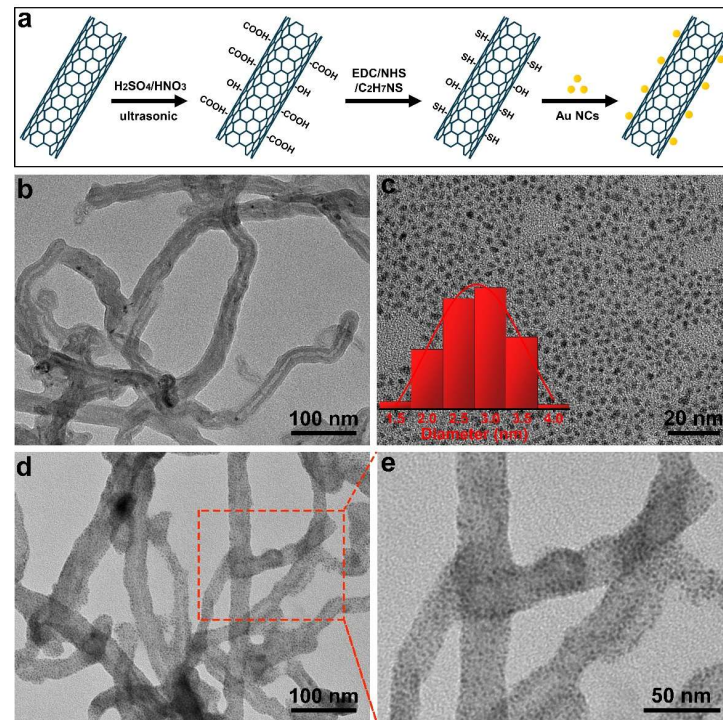


Figure 1. (a) Schematic illustration of the synthesis of MWCNTs@Au NCs. TEM images of (b) MWCNTs, (c) Au NCs (the inset depicts the size distribution of Au NCs) and (d,e) MWCNTs@Au NCs.

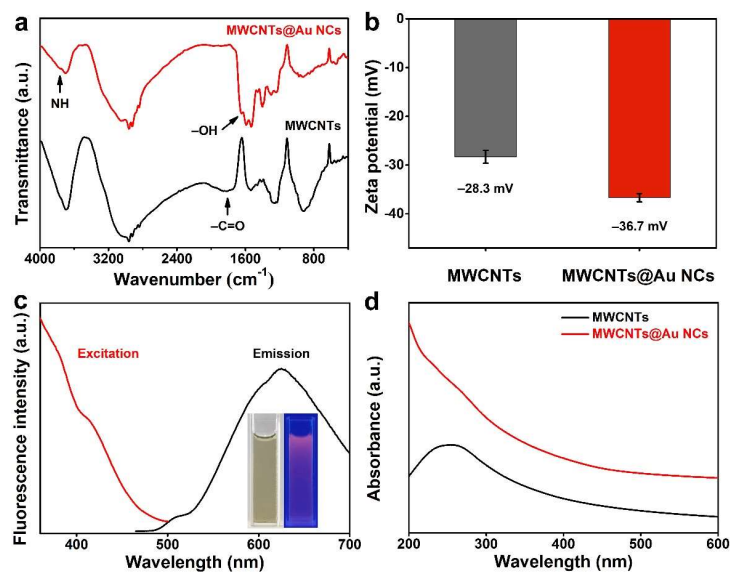


Figure 2. (a) FTIR spectra and (b) zeta potentials of MWCNTs and MWCNTs@Au NCs. (c) Fluorescence excitation and emission spectra of MWCNTs@Au NCs (the inset shows the optical photographs of MWCNTs@Au NCs under sunlight (left) and 360 nm UV light (right)). (d) UV–vis absorption spectra of MWCNTs and MWCNTs@Au NCs.

3.2. Detection Principle of miR-92a-3p

As depicted in Figure 3a, in the absence of miR-92a-3p, single-stranded DNA probes are adsorbed on the surface of MWCNTs@Au NCs, and the fluorescence of Atto-425 is quenched. When miR-92a-3p appears, the probe–miR-92a-3p hybrid duplex is formed and leaves from MWCNTs@Au NCs. The fluorescence of Atto-425 is thus recovered. Then, the probe in the duplex is cleaved by DSN and subsequently miR-92a-3p is released to participate in the next hybridization to form a signal amplification cycle. Therefore, the fluorescence intensity of Atto-425 is positively correlated with the concentration of miR-92a-3p, while the fluorescence intensity of Au NCs remains stable. In theory, the concentration of miR-92a-3p is positively correlated with the Δ Atto-425/Au NCs fluorescence intensity ratio.

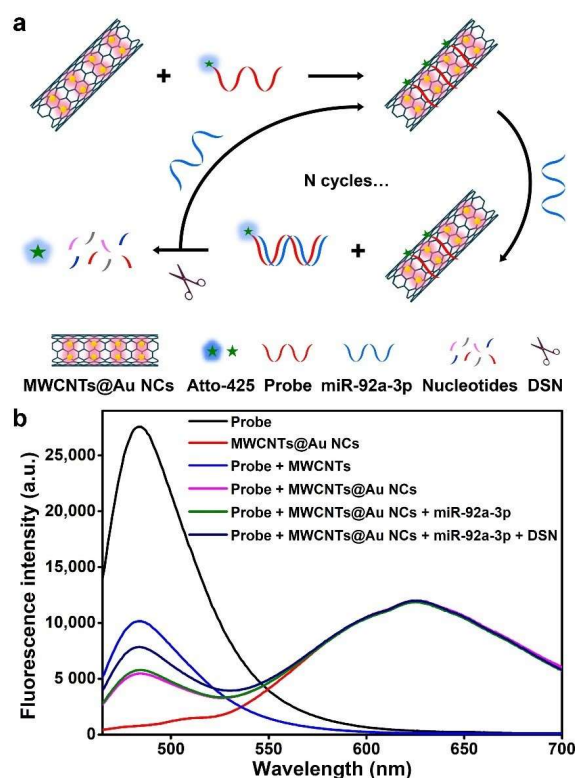


Figure 3. (a) Schematic diagram of fluorescence detection of miR-92a-3p based on MWCNTs@Au NCs and DSN-assisted signal amplification. (b) Fluorescence spectra of probe, MWCNTs@Au NCs, probe + MWCNTs, probe + MWCNTs@Au NCs, probe + MWCNTs@Au NCs + miR-92a-3p, and probe + MWCNTs@Au NCs + miR-92a-3p + DSN.

The fluorescence signals of different material systems were measured to evaluate the feasibility of the biosensing (Figure 3b). The fluorescence peak of Atto-425 is located at 482 nm and is 143 nm away from that of Au NCs, which avoids interference of the two fluorescent materials with each other. MWCNTs@Au NCs show stronger fluorescence quenching than MWCNTs, which is attributed to the enhanced effect of the fluorescence quenching capability of Au NCs [42,43]. The addition of 1 pM miR-92a-3p results in a slight recovery of the fluorescence of Atto-425, which is attributed to the formation of the probe–miR-92a-3p hybrid duplex. The addition of DSN results in more pronounced fluorescence recovery of Atto-425 in the presence of 1 pM miR-92a-3p, demonstrating the feasibility of the DSN-assisted signal amplification strategy. Therefore, the proposed ratiometric fluorescent biosensor can be used for sensitive detection of miR-92a-3p.

3.3. Optimization of Measurement Conditions

The effect of the amount of MWCNTs@Au NCs on the fluorescence signals of the biosensing system was investigated. As shown in Figure 4a, the fluorescence of Atto-425

decreases with the increase of MWCNTs@Au NCs. When the amount of MWCNTs@Au NCs is increased from 0.028 mg/mL to 0.035 mg/mL, the decrease in the fluorescence intensity of Atto-425 slows down. So, 0.035 mg/mL MWCNTs@Au NCs aqueous solution is determined as optimal. Variation of the fluorescence intensity of Atto-425 with the mixing time of the probe and MWCNTs@Au NCs was investigated to determine the time required to achieve stable adsorption and quenching (Figure 4b). Within 10 min of mixing, the fluorescence of Atto-425 decreases significantly. The fluorescence intensity of Atto-425 decreases sharply at 10–20 min, indicating that a large number of probes are adsorbed on the surface of MWCNTs@Au NCs. A slight decrease in the fluorescence intensity is observed at 30–40 min, indicating that most of the probes are adsorbed on the surface of MWCNTs@Au NCs within 40 min. Therefore, 40 min is selected as the optimal mixing time. The activity of DSN and hybridization between complementary single-stranded nucleic acids are significantly affected by the incubation temperature [41]. Therefore, the effect of incubation temperature on the fluorescence signals of the biosensing system at a miR-92a-3p concentration of 1 pM was investigated. As shown in Figure 4c, the maximum $(F-F_0)_{482}/F_{625}$ value is obtained at 45 °C, while a lower or higher temperature results in a decreased $(F-F_0)_{482}/F_{625}$ value due to inefficient hybridization between probe and miR-92a-3p or reduction in the activity of DSN [44]. Thus, 45 °C is determined to be the optimal incubation temperature.

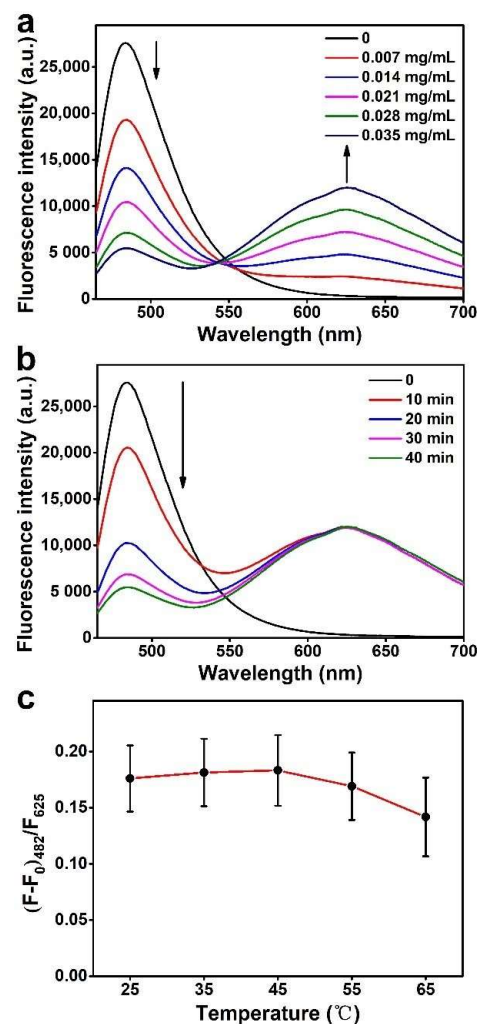


Figure 4. (a) The effect of the amount of MWCNTs@Au NCs on the fluorescence signals of the biosensing system. (b) The variation of the fluorescence of Atto-425 with the mixing time of the probe and MWCNTs@Au NCs. (c) The effect of incubation temperature on the fluorescence signals ($n = 3$, mean \pm s.d.).

3.4. Sensitivity and Selectivity for miR-92a-3p Detection

The sensitivity of the proposed biosensor to miR-92a-3p was measured under optimized conditions. Figure 5a–b show that the fluorescence intensity of Atto-425 linearly increases along with the increase of miR-92a-3p concentration from 0.1 to 10 pM, and a calculated detection limit of 31 fM is obtained based on 3σ . The goodness-of-fit of the regression equation is 0.996, indicating that the biosensor shows excellent regularity and stability. Compared to previously reported ratiometric fluorescent biosensors and DSN signal amplification-based fluorescent biosensors enumerated in Table 2, our fabricated biosensor exhibits a satisfactory linear detection interval and detection limit, demonstrating its potential for sensitive detection of miRNAs. In addition, to evaluate detection selectivity, concentration assays were performed with SMT, TMT and NCT as control targets. The pre-set concentration of all sequences was 1 pM, and the fluorescence signals they produced are presented in Figure 5c. The $(F-F_0)_{482}/F_{625}$ values corresponding to mismatched sequences are significantly lower than that of miR-92a-3p, indicating that mismatched sequences cannot give rise to efficient fluorescence recovery of Atto-425. According to the regression equation, the measured concentrations of SMT, TMT and NCT are 0.16, 0.15 and 0.13 pM, respectively, which are much lower than their actual concentrations. This indicates the proposed biosensor can selectively detect miR-92a-3p.

Table 2. Comparison of the detection performance of the ratiometric fluorescent biosensors and DSN signal amplification-based fluorescent biosensors for miRNAs.

Fluorescent Materials	Targets	Linear Interval (pM)	Limit of Detection (pM)	Ref.
DNA-AgNCs	miR-141	5×10^3 – 1×10^5	2.5×10^3	[45]
Protonated phenyl-doped carbon nitride, ROX	miRNA-224	10^3 – 2×10^4	200	[46]
FAM, TAMRA	miRNA-21	10^2 – 2×10^4	73	[47]
NMM, DAPI	miRNA-21	10 – 4.5×10^4	3.1	[48]
Chameleon Ag NCs	miR-17-5p	10 – 10^4	2.8	[49]
CDs, FAM	miRNA-21	50 – 10^4	1	[50]
CdTe QDs, FCMMs	let-7a	2 – 2×10^2	0.1	[13]
Boron doped g-C ₃ N ₄ nanosheets, Cu NCs	miR-582-3p	0.2–1	0.049	[25]
FAM	let-7a	0.5 – 5×10^2	0.4	[51]
FAM	miRNA-21	0.1 – 1×10^3	0.1	[52]
FAM	let-7b	0.5 – 10^3	0.16	[53]
FAM	miRNA-141	5 – 10^3	0.42	[54]
FAM	let-7a	0.1 – 2×10^3	0.06	[55]
Hairpin structure molecular beacons	let-7a	1 – 10^4	0.0325	[56]
MWCNTs@Au NCs, Atto-425	miR-92a-3p	0.1–10	0.031	This work

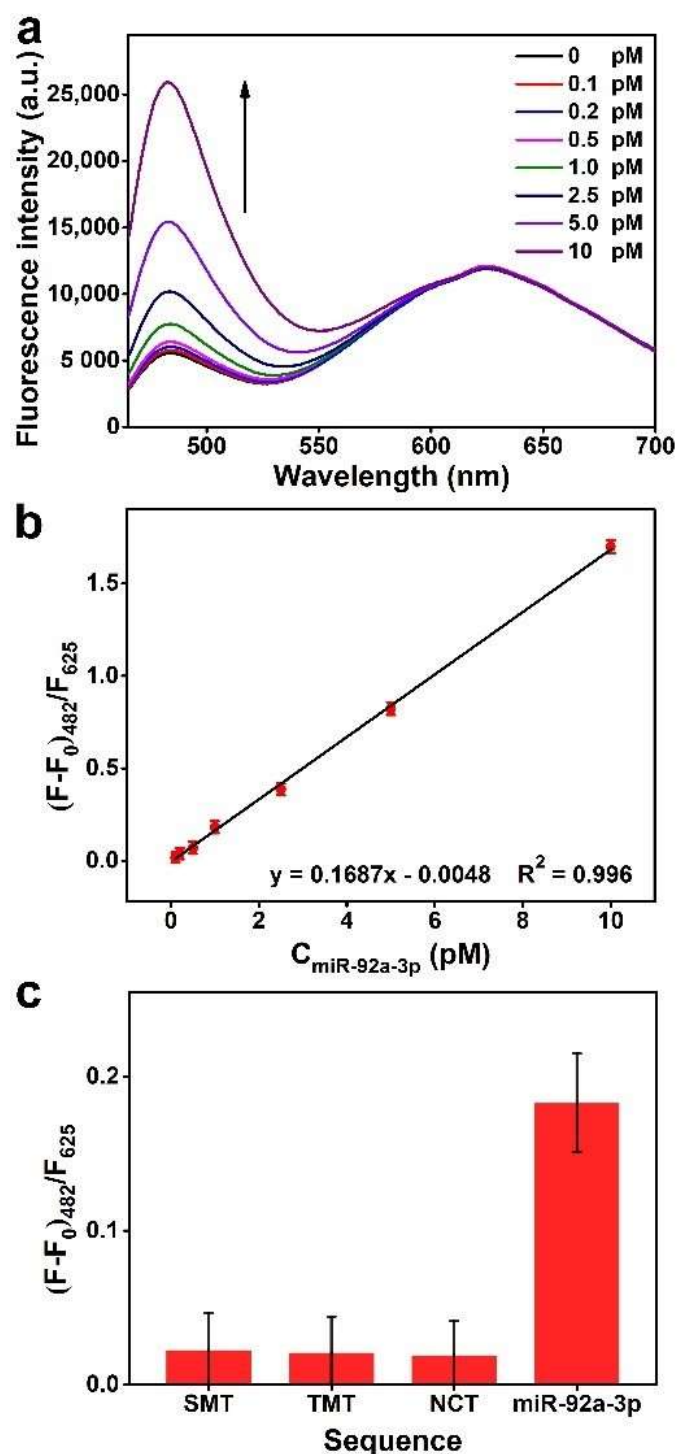


Figure 5. (a) Fluorescence spectra of the biosensor under different concentrations of miR-92a-3p. (b) The calibration line of the Δ probe/MWCNTs@Au NCs fluorescence ratio against the concentration of miR-92a-3p ($n = 3$, mean \pm s.d.). (c) Comparison of the fluorescence signals produced by miR-92a-3p and mismatched sequences ($n = 3$, mean \pm s.d.).

3.5. Detection of miR-92a-3p Extracted from Exosomes

Before performing the exosomal miR-92a-3p assay, exosomes were extracted from human serum, and their internal miR-92a-3p was obtained by cleaving the exosomes. At first, the morphology of exosomes was characterized by the TEM. They are spherical and exhibit dimensions in the range of 30–110 nm (Figure 6a). According to the literature,

exosomes may shrink during TEM sample preparation, which results in the observed size of exosomes being smaller than their actual size [57]. Furthermore, exosomes extracted from three CRC patients and three healthy controls were identified by Western blotting to demonstrate their successful extraction. The marker proteins of exosomes, CD63 and CD9 were detected [58,59]. From Figure 6b, Western blotting images demonstrate that there are abundant CD63 and CD9 in exosomes. The significant binding in exosome-enriched samples validates the efficient extraction of exosomes.

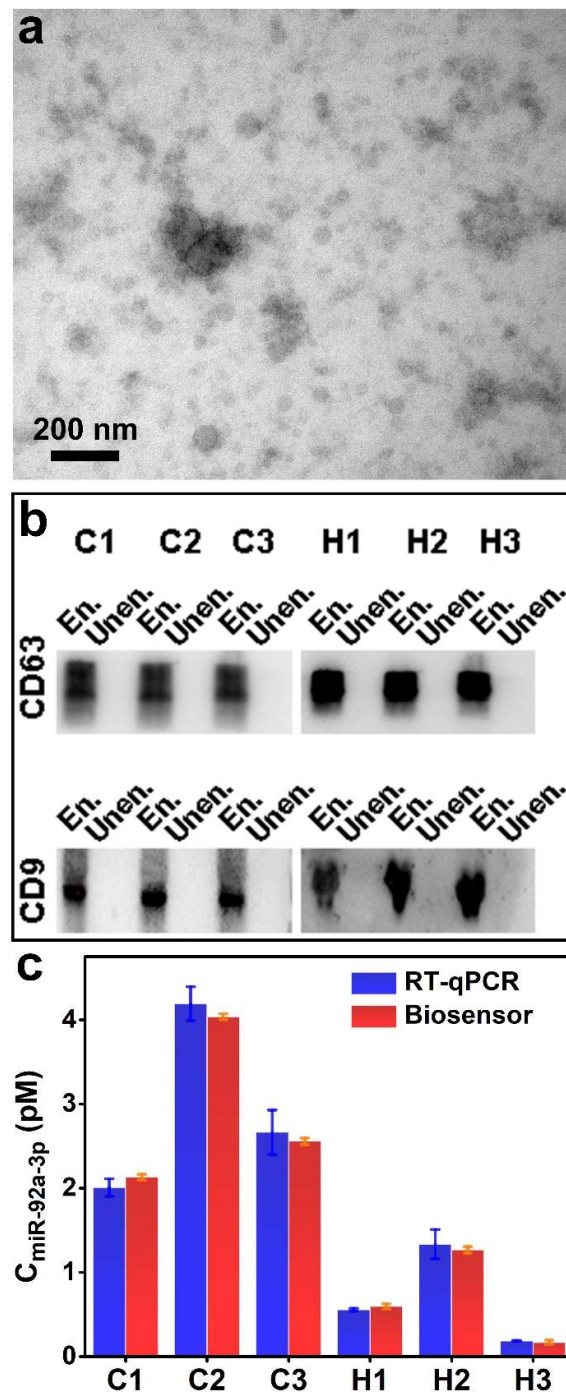


Figure 6. (a) TEM image of exosomes. (b) Western blotting of exosome-enriched (En.) and exosome-unenriched (Unen.) samples. C1~C3 represent CRC patients; H1~H3 represent healthy controls. (c) Comparison of the concentration of exosomal miR-92a-3p of three CRC patients and three healthy controls detected by RT-qPCR and the proposed biosensor ($n = 3$, mean \pm s.d.).

To verify the accuracy of our fabricated biosensor, RT-qPCR and the ratiometric fluorescent biosensor were used in parallel to detect the concentration of miR-92a-3p extracted from exosomes. As shown in Figure 6c, the detection results of the ratiometric fluorescent biosensor are consistent with those of RT-qPCR, demonstrating that our fabricated biosensor possesses high accuracy and practicality. In addition, the detection results of the ratiometric fluorescent biosensor showed higher stability than RT-qPCR. Furthermore, due to the sequence modification flexibility of the probe, other RNAs can also be detected by this biosensor by simply changing the probe sequence.

4. Conclusions

In conclusion, a ratiometric fluorescent biosensor based on MWCNTs@Au NCs and DSN-assisted signal amplification was fabricated for the detection of CRC-associated miR-92a-3p extracted from exosomes. Because of the fluorescence reference capability of MWCNTs@Au NCs, this biosensor is stable enough to detect clinical samples. With the introduction of DSN-assisted signal amplification, this biosensor exhibits high sensitivity and a limit of detection as low as 31 fM. Furthermore, the specific cleavage characteristic of DSN endows this biosensor with high selectivity, even against single-base mismatched targets. Furthermore, because of the flexibility of sequence modification, this biosensor is able to detect other RNAs by simply changing the sequence of the probe. In view of these advantages, our fabricated ratiometric fluorescent biosensor shows the possibility of achieving early diagnosis for diseases by detecting miRNAs.

Author Contributions: Conceptualization, Y.J., L.D. and Z.S.; methodology, Z.S. and J.L.; formal analysis, Y.T., L.Z. and X.Z.; investigation, Z.S., J.L. and Y.T.; resources, Y.J., L.D., H.L. and C.W.; data curation, Z.S. and Y.T.; writing—original draft preparation, Z.S., J.L. and Y.T.; writing—review and editing, Y.J. and L.D.; supervision, Y.J., L.D., H.L. and C.W.; funding acquisition, Y.J. and H.L. All authors have read and agreed to the published version of the manuscript.

Funding: This work was financially supported by the National Natural Science Foundation of China (grants no. 52101287 and U1806219), the Shenzhen Fundamental Research Program (grant no. JCYJ20190807092803583), the Natural Science Foundation of Jiangsu Province (grant no. BK20190205) and the Basic and Applied Basic Research Foundation of Guangdong Province (grant no. 2019A1515110846). This work was also supported by the special fund of the Project of the Qilu Young Scholar Program of Shandong University.

Institutional Review Board Statement: This work was approved by the ethics committee of the Second Hospital of Shandong University (project number: KYLL-2019(KJ)P-0067).

Informed Consent Statement: Informed consent was obtained from all subjects involved in the study.

Data Availability Statement: Not applicable.

Conflicts of Interest: The authors declare no conflict of interest.

References

1. Kilikevicius, A.; Meister, G.; Corey, D.R. Reexamining assumptions about miRNA-guided gene silencing. *Nucleic Acids Res.* **2022**, *50*, 617–634. [[CrossRef](#)] [[PubMed](#)]
2. Kunze-Schumacher, H.; Krueger, A. The Role of MicroRNAs in Development and Function of Regulatory T Cells—Lessons for a Better Understanding of MicroRNA Biology. *Front. Immunol.* **2020**, *11*, 2185. [[CrossRef](#)] [[PubMed](#)]
3. Yang, H.; Chen, J.B.; Yang, S.; Zhang, T.; Xia, X.H.; Zhang, K.X.; Deng, S.; He, G.P.; Gao, H.; He, Q.; et al. CRISPR/Cas14a-Based Isothermal Amplification for Profiling Plant MicroRNAs. *Anal. Chem.* **2021**, *93*, 12602–12608. [[CrossRef](#)] [[PubMed](#)]
4. Zhang, G.Q.; Wang, S.Q.; Chen, Y.; Fu, L.Y.; Xu, Y.N.; Li, L.; Tao, L.; Shen, X.C. MicroRNAs Regulating Mitochondrial Function in Cardiac Diseases. *Front. Pharmacol.* **2021**, *12*, 663322. [[CrossRef](#)] [[PubMed](#)]
5. Murri, M.; Insenser, M.; Fernandez-Duran, E.; San-Millan, J.L.; Escobar-Morreale, H.F. Effects of Polycystic Ovary Syndrome (PCOS), Sex Hormones, and Obesity on Circulating miRNA-21, miRNA-27b, miRNA-103, and miRNA-155 Expression. *J. Clin. Endocrinol. Metab.* **2013**, *98*, E1835–E1844. [[CrossRef](#)]
6. He, X.Y.; Kuang, G.Y.; Wu, Y.R.; Ou, C.L. Emerging roles of exosomal miRNAs in diabetes mellitus. *Clin. Transl. Med.* **2021**, *11*, e468. [[CrossRef](#)] [[PubMed](#)]

7. Singh, S.; Raza, W.; Parveen, S.; Meena, A.; Luqman, S. Flavonoid display ability to target microRNAs in cancer pathogenesis. *Biochem. Pharmacol.* **2021**, *189*, 114409. [[CrossRef](#)]
8. Chakraborty, C.; Sharma, A.R.; Sharma, G.; Lee, S.S. Therapeutic advances of miRNAs: A preclinical and clinical update. *J. Adv. Res.* **2021**, *28*, 127–138. [[CrossRef](#)]
9. Wu, Y.; Zhang, Y.; Zhang, X.H.; Luo, S.H.; Yan, X.H.; Qiu, Y.R.; Zheng, L.; Li, L. Research advances for exosomal miRNAs detection in biosensing: From the massive study to the individual study. *Biosens. Bioelectron.* **2021**, *177*, 112962. [[CrossRef](#)]
10. Zhu, D.; Miao, Z.Y.; Hu, Y.; Zhang, X.J. Single-step, homogeneous and sensitive detection for microRNAs with dual-recognition steps based on luminescence resonance energy transfer (LRET) using upconversion nanoparticles. *Biosens. Bioelectron.* **2018**, *100*, 475–481. [[CrossRef](#)]
11. Wijesinghe, K.M.; Kanak, M.A.; Harrell, J.C.; Dhakal, S. Single-Molecule Sensor for High-Confidence Detection of miRNA br. *ACS Sens.* **2022**, *7*, 1086–1094. [[CrossRef](#)] [[PubMed](#)]
12. Hu, C.Y.; Zhang, L.L.; Yang, Z.Z.; Song, Z.; Zhang, Q.; He, Y. Graphene oxide-based qRT-PCR assay enables the sensitive and specific detection of miRNAs for the screening of ovarian cancer. *Anal. Chim. Acta* **2021**, *1174*, 338715. [[CrossRef](#)] [[PubMed](#)]
13. Zhang, W.Y.; Hao, W.H.; Liu, X.T.; Sun, X.R.; Yan, J.L.; Wang, Y.C. Visual detection of miRNAs using enzyme-free amplification reactions and ratiometric fluorescent probes. *Talanta* **2020**, *219*, 121332. [[CrossRef](#)] [[PubMed](#)]
14. Xia, Y.K.; Wang, L.L.; Li, J.; Chen, X.Q.; Lan, J.M.; Yan, A.; Lei, Y.; Yang, S.; Yang, H.H.; Chen, J.H. A Ratiometric Fluorescent Bioprobe Based on Carbon Dots and Acridone Derivate for Signal Amplification Detection Exosomal microRNA. *Anal. Chem.* **2018**, *90*, 8969–8976. [[CrossRef](#)] [[PubMed](#)]
15. Zhu, S.; Yang, Y.Q.; Ding, Y.D.; Feng, N.H.; Li, M.L.; Yin, Y.M. Engineering entropy-driven based multiple signal amplification strategy for visualized assay of miRNA by naked eye. *Talanta* **2021**, *235*, 122810. [[CrossRef](#)] [[PubMed](#)]
16. Liu, L.; Deng, D.H.; Wu, D.H.; Hou, W.L.; Wang, L.; Li, N.; Sun, Z.F. Duplex-specific nuclease-based electrochemical biosensor for the detection of microRNAs by conversion of homogeneous assay into surface-tethered electrochemical analysis. *Anal. Chim. Acta* **2021**, *1149*, 338199. [[CrossRef](#)]
17. Yin, B.C.; Liu, Y.Q.; Ye, B.C. One-step, multiplexed fluorescence detection of microRNAs based on duplex-specific nuclease signal amplification. *J. Am. Chem. Soc.* **2012**, *134*, 5064–5067. [[CrossRef](#)]
18. Liu, Q.; Kang, P.J.; Chen, Z.P.; Shi, C.X.; Chen, Y.; Yu, R.Q. Highly specific and sensitive detection of microRNAs by tandem signal amplification based on duplex-specific nuclease and strand displacement. *Chem. Commun.* **2019**, *55*, 14210–14213. [[CrossRef](#)]
19. Yu, L.; He, P.; Xu, Y.C.; Kou, X.Y.; Yu, Z.Q.; Xie, X.B.; Miao, P. Manipulations of DNA four-way junction architecture and DNA modified Fe₃O₄@Au nanomaterials for the detection of miRNA. *Sens. Actuator B-Chem.* **2020**, *313*, 128015. [[CrossRef](#)]
20. Wu, Y.D.; Cui, S.; Li, Q.; Zhang, R.S.; Song, Z.M.; Gao, Y.Z.; Chen, W.J.; Xing, D.M. Recent advances in duplex-specific nuclease-based signal amplification strategies for microRNA detection. *Biosens. Bioelectron.* **2020**, *165*, 112449. [[CrossRef](#)]
21. Wang, S.; Zhang, L.Y.; Kan, A.L.; Xu, X.W.; Zhang, N.; Jiang, W. MnO₂ nanosheet-mediated target-binding-induced FRET strategy for multiplexed microRNAs detection and imaging in living cells. *Talanta* **2021**, *226*, 122202. [[CrossRef](#)] [[PubMed](#)]
22. Sun, Z.W.; Tong, Y.; Zhou, X.Y.; Li, J.; Zhao, L.; Li, H.; Wang, C.X.; Du, L.T.; Jiang, Y.Y. Ratiometric Fluorescent Biosensor Based on Forster Resonance Energy Transfer between Carbon Dots and Acridine Orange for miRNA Analysis. *ACS Omega* **2021**, *6*, 34150–34159. [[CrossRef](#)] [[PubMed](#)]
23. Zhang, Q.X.; Wang, F.; Zhang, H.X.; Zhang, Y.Y.; Liu, M.L.; Liu, Y. Universal Ti₃C₂ MXenes Based Self-Standard Ratiometric Fluorescence Resonance Energy Transfer Platform for Highly Sensitive Detection of Exosomes. *Anal. Chem.* **2018**, *90*, 12737–12744. [[CrossRef](#)]
24. Lee, J.S.; Kim, J.; Shin, H.; Min, D.H. Graphene oxide-based molecular diagnostic biosensor for simultaneous detection of Zika and dengue viruses. *2D Mater.* **2020**, *7*, 044001. [[CrossRef](#)]
25. Wang, Y.T.; Wu, N.; Guo, F.N.; Gao, R.X.; Yang, T.; Wang, J.H. g-C₃N₄ nanosheet-based ratiometric fluorescent probes for the amplification and imaging of miRNA in living cells. *J. Mat. Chem. B* **2019**, *7*, 7566–7573. [[CrossRef](#)] [[PubMed](#)]
26. Oudeng, G.; Au, M.T.; Shi, J.Y.; Wen, C.Y.; Yang, M. One-Step in Situ Detection of miRNA-21 Expression in Single Cancer Cells Based on Biofunctionalized MoS₂ Nanosheets. *ACS Appl. Mater. Interfaces* **2018**, *10*, 350–360. [[CrossRef](#)] [[PubMed](#)]
27. Zhao, Q.; Piao, J.F.; Peng, W.P.; Wang, Y.; Zhang, B.; Gong, X.Q.; Chang, J. Simple and Sensitive Quantification of MicroRNAs via PS@Au Microspheres-Based DNA Probes and DSN-Assisted Signal Amplification Platform. *ACS Appl. Mater. Interfaces* **2018**, *10*, 3324–3332. [[CrossRef](#)]
28. Li, X.T.; Tang, X.M.; Chen, X.J.; Qu, B.H.; Lu, L.H. Label-free and enzyme-free fluorescent isocarboxyphos aptasensor based on MWCNTs and G-quadruplex. *Talanta* **2018**, *188*, 232–237. [[CrossRef](#)]
29. Ding, Z.Q.; Bligh, S.W.A.; Tao, L.; Quan, J.; Nie, H.L.; Zhu, L.M.; Gong, X. Molecularly imprinted polymer based on MWCNT-QDs as fluorescent biomimetic sensor for specific recognition of target protein. *Mater. Sci. Eng. C-Mater. Biol. Appl.* **2015**, *48*, 469–479. [[CrossRef](#)]
30. Ma, H.; Xue, N.; Li, Z.B.; Xing, K.; Miao, X.M. Ultrasensitive detection of miRNA-155 using multi-walled carbon nanotube-gold nanocomposites as a novel fluorescence quenching platform. *Sens. Actuator B-Chem.* **2018**, *266*, 221–227. [[CrossRef](#)]

31. Reddu, V.; Sun, L.; Li, X.; Jin, H.; Wang, S.; Wang, X. Highly selective and efficient electroreduction of CO₂ in water by quaterpyridine derivative-based molecular catalyst noncovalently tethered to carbon nanotubes. *SmartMat* **2022**, *3*, 151–162. [[CrossRef](#)]
32. Dong, P.; Liu, Y.H.; Zhao, Y.; Wang, W.X.; Pan, M.; Liu, Y.; Liu, X.Q. Ratiometric fluorescence sensing of copper ion and enzyme activity by nanoprobe-mediated autocatalytic reaction and catalytic cascade reaction. *Sens. Actuator B-Chem.* **2020**, *310*, 127873. [[CrossRef](#)]
33. Jia, P.; Yang, J.Y.; Hou, J.J.; Yang, K.R.; Zhe, T.T.; Bu, T.; Wang, L. Innovative ratiometric optical strategy: Nonconjugated polymer dots based fluorescence-scattering dual signal output for sensing mercury ions. *Food Chem.* **2022**, *374*, 131771. [[CrossRef](#)] [[PubMed](#)]
34. Han, Y.P.; Zou, R.; Wang, L.Y.; Chen, C.Y.; Gong, H.; Cai, C.Q. An amine-functionalized metal-organic framework and triple-helix molecular beacons as a sensing platform for miRNA ratiometric detection. *Talanta* **2021**, *228*, 122199. [[CrossRef](#)] [[PubMed](#)]
35. Liu, J.S.; Fu, T.; Wu, F.F.; Wang, H.X. Ratiometric fluorescence and smartphone dual-mode detection of glutathione using carbon dots coupled with Ag⁺-triggered oxidation of o-phenylenediamine. *Nanotechnology* **2021**, *32*, 445501. [[CrossRef](#)]
36. Fan, Y.Y.; Deng, X.; Wang, M.; Li, J.; Zhang, Z.Q. A dual-function oligonucleotide-based ratiometric fluorescence sensor for ATP detection. *Talanta* **2020**, *219*, 121349. [[CrossRef](#)]
37. Hu, J.L.; Wang, W.; Lan, X.L.; Zeng, Z.C.; Liang, Y.S.; Yan, Y.R.; Song, F.Y.; Wang, F.F.; Zhu, X.H.; Liao, W.J.; et al. CAFs secreted exosomes promote metastasis and chemotherapy resistance by enhancing cell stemness and epithelial-mesenchymal transition in colorectal cancer. *Mol. Cancer* **2019**, *18*, 91. [[CrossRef](#)]
38. Misak, H.E.; Asmatulu, R.; O'Malley, M.; Jurak, E.; Mall, S. Functionalization of carbon nanotube yarn by acid treatment. *Int. J. Smart Nano Mater.* **2014**, *5*, 34–43. [[CrossRef](#)]
39. Jing, P.J.; Yin, Z.Z.; Cai, W.R.; Li, J.Y.; Wu, D.T.; Kong, Y. The hybrids of perylene tetracarboxylic acid functionalized multi-walled carbon nanotubes and chitosan for electrochemical chiral sensing of tryptophan enantiomers. *Bioelectrochemistry* **2022**, *146*, 108110. [[CrossRef](#)]
40. Parida, K.M.; Sahu, N.; Tripathi, A.K.; Kamble, V.S. Gold Promoted S,N-Doped TiO₂: An Efficient Catalyst for CO Adsorption and Oxidation. *Environ. Sci. Technol.* **2010**, *44*, 4155–4160. [[CrossRef](#)]
41. Kim, D.; Kim, Y. Extinction Effect of Gold Nanocatalysts on Photocatalytic Activities under Plasmonic Excitation. *Catalysts* **2021**, *11*, 413. [[CrossRef](#)]
42. Yang, W.T.; Shen, Y.; Zhang, D.Y.; Li, C.; Yuan, R.; Xu, W.J. Programmed Dual-Functional DNA Tweezer for Simultaneous and Recognizable Fluorescence Detection of microRNA and Protein. *Anal. Chem.* **2019**, *91*, 7782–7789. [[CrossRef](#)] [[PubMed](#)]
43. Du, X.Y.; Wu, S.H.; Huang, X.B.; Sun, J.J. Ag Nanocubes Coupled with Heating-Enhanced DSN-Assisted Cycling Amplification for Surface-Enhanced Raman Spectroscopy Detection of MicroRNA-21. *ACS Appl. Nano Mater.* **2021**, *4*, 2565–2574. [[CrossRef](#)]
44. Liu, M.Q.; Shen, R.; Li, H.R.; Jia, Y.W.; Mak, P.I.; Martins, R.P. Ratiometric fluorescence analysis for miR-141 detection with hairpin DNA-templated silver nanoclusters. *J. Mater. Chem. C* **2022**, *10*, 655–664. [[CrossRef](#)]
45. Huang, J.; Shangguan, J.F.; Guo, Q.P.; Ma, W.J.; Wang, H.Z.; Jia, R.C.; Ye, Z.; He, X.X.; Wang, K.M. Colorimetric and fluorescent dual-mode detection of microRNA based on duplex-specific nuclease assisted gold nanoparticle amplification. *Analyst* **2019**, *144*, 4917–4924. [[CrossRef](#)]
46. Zhou, D.S.; Liu, X.T.; Liu, X.T.; Xu, Y.T.; Chen, R.Q.; Lin, C.; Guo, L.Q.; Fu, F.F. Ratiometric fluorescent biosensor for microRNAs imaging in living cells. *Sens. Actuator B-Chem.* **2020**, *322*, 128632. [[CrossRef](#)]
47. Wang, S.; Wang, L.; Xu, X.W.; Li, X.; Jiang, W. MnO₂ nanosheet-mediated ratiometric fluorescence biosensor for MicroRNA detection and imaging in living cells. *Anal. Chim. Acta* **2019**, *1063*, 152–158. [[CrossRef](#)]
48. Ji, D.Y.; Mou, X.; Kwok, C.K. Label-free and ratiometric detection of microRNA based on target-induced catalytic hairpin assembly and two fluorescent dyes. *Anal. Methods* **2019**, *11*, 4808–4813. [[CrossRef](#)]
49. Jiang, Y.T.; Ma, X.Y.; Shao, X.J.; Wang, M.Y.; Jiang, Y.; Miao, P. Chameleon silver nanoclusters for ratiometric sensing of miRNA. *Sens. Actuator B-Chem.* **2019**, *297*, 126788. [[CrossRef](#)]
50. Wang, Z.Z.; Xue, Z.Q.; Hao, X.L.; Miao, C.F.; Zhang, J.Z.; Zheng, Y.J.; Zheng, Z.F.; Lin, X.H.; Weng, S.H. Ratiometric fluorescence sensor based on carbon dots as internal reference signal and T7 exonuclease-assisted signal amplification strategy for microRNA-21 detection. *Anal. Chim. Acta* **2020**, *1103*, 212–219. [[CrossRef](#)]
51. Lin, X.Y.; Zhang, C.; Huang, Y.S.; Zhu, Z.; Chen, X.; Yang, C.J. Backbone-modified molecular beacons for highly sensitive and selective detection of microRNAs based on duplex specific nuclease signal amplification. *Chem. Commun.* **2013**, *49*, 7243–7245. [[CrossRef](#)] [[PubMed](#)]
52. Sun, C.H.; Rong, Y.; Yang, Z.P.; She, D.; Gong, M.W. Construction of Dual-Target Recognition-Based Specific MicroRNA Detection Method for Acute Pancreatitis Analysis. *Appl. Biochem. Biotechnol.* **2022**, *194*, 3136–3144. [[CrossRef](#)] [[PubMed](#)]
53. Guo, S.; Yang, F.; Zhang, Y.L.; Ning, Y.; Yao, Q.F.; Zhang, G.J. Amplified fluorescence sensing of miRNA by combination of graphene oxide with duplex-specific nuclease. *Anal. Methods* **2014**, *6*, 3598–3603. [[CrossRef](#)]
54. Sun, Y.J.; Wang, C.C.; Tang, L.N.; Zhang, Y.L.; Zhang, G.J. Magnetic-enhanced fluorescence sensing of tumor miRNA by combination of MNPs@PDA with duplex specific nuclease. *RSC Adv.* **2021**, *11*, 2968–2975. [[CrossRef](#)]

55. Shen, W.; Yeo, K.H.; Gao, Z.Q. A simple and highly sensitive fluorescence assay for microRNAs. *Analyst* **2015**, *140*, 1932–1938. [[CrossRef](#)] [[PubMed](#)]
56. Yao, G.D.; Xiao, Z.Y.; Yu, S.; Yao, K.; Liu, D.H.; Chen, K.X.; Wei, Z.M.; Li, Y.J.; Sun, F.F. Tetrahedral structure supported two stages DSN-assisted amplification strategy for sensitive detection of lung cancer related MicroRNA. *Microchem. J.* **2022**, *174*, 107035. [[CrossRef](#)]
57. Zhang, W.; Peng, P.; Kuang, Y.; Yang, J.X.; Cao, D.Y.; You, Y.; Shen, K. Characterization of exosomes derived from ovarian cancer cells and normal ovarian epithelial cells by nanoparticle tracking analysis. *Tumor Biol.* **2016**, *37*, 4213–4221. [[CrossRef](#)]
58. Sun, Z.W.; Yang, J.J.; Li, H.; Wang, C.X.; Fletcher, C.; Li, J.; Zhan, Y.; Du, L.T.; Wang, F.L.; Jiang, Y.Y. Progress in the research of nanomaterial-based exosome bioanalysis and exosome-based nanomaterials tumor therapy. *Biomaterials* **2021**, *274*, 120873. [[CrossRef](#)]
59. Liu, H.Y.; Liu, W.; Jin, G. Detection of Exosomes Using Total Internal Reflected Imaging Ellipsometry. *Biosensors* **2021**, *11*, 164. [[CrossRef](#)]